Manuscript details

Manuscript number	IE_2016_34
Title	Development and validation of a set-up to measure the transferred multi-axial impact momentum of a bird strike on a booster vane
Article type	Research Paper

Abstract

Reaction force has always been one of the main characterization parameters for impact events. Today, a set of force transducers are a common and valuable tool to measure reaction forces. But the force signals are often influenced by vibrations of the supporting structures. Many other attempts were already taken in the past to use other methods to measure force, such as ballistic pendulums, Hopkinson bars, etc., all having their advantages and disadvantages. In this work, a multi-axial force measurement tool is developed to serve in a test campaign of bird strike experiments on booster vanes. The idea is to give some well-chosen mass three rotational degrees of freedom and acquire the transferred rotational momentum from an optical measurement, which is a direct measure for the impact force. The tool is validated experimentally and numerically using a simplified steel vane.

Keywords Force measurements; impact; bird strike; numerical simulation

Corresponding Author Frederik Allaeys

Corresponding Author's Institution Ghent University

Order of Authors Frederik Allaeys, Geert Luyckx, Wim Van Paepegem, Joris Degrieck

Submission files included in this PDF

File Type	File Name
Manuscript File	Paper multi axial impact momentum measurement - submit.

Development and validation of a set-up to measure the transferred multi-axial impact momentum of a bird strike on a booster vane

Frederik Allaeys[1], Geert Luyckx[1], Wim Van Paepegem[1] and Joris Degrieck[1]

[1]Department of Material Science and Engineering,

Ghent University, Technologiepark 903, 9052 Zwijnaarde, Belgium

Frederik.allaeys@UGent.be

Abstract

Reaction force has always been one of the main characterization parameters for impact events. Today, a set of force transducers are a common and valuable tool to measure reaction forces. But the force signals are often influenced by vibrations of the supporting structures. Many other attempts were already taken in the past to use other methods to measure force, such as ballistic pendulums, Hopkinson bars, etc., all having their advantages and disadvantages. In this work, a multi-axial force measurement tool is developed to serve in a test campaign of bird strike experiments on booster vanes. The idea is to give some well-chosen mass three rotational degrees of freedom and acquire the transferred rotational momentum from an optical measurement, which is a direct measure for the impact force. The tool is validated experimentally and numerically using a simplified steel vane.

Keywords: Force measurements, impact, bird strike, numerical simulation

1) Introduction

Certification by analysis is a hot topic these days. But, a lot of research is still required to be able to prove that numerical methods are fully capable for simulating bird strike. The work described in this paper is part of the European FP7 project *E-Break* or *Engine BREAKthrough Components and Subsystems*, where the key jet engine subsystem technologies are further developed to incorporate in ultra-high overall pressure ratio (OPR) and high bypass ratio (BPR) engines. In this project, a small task is devoted to the development of a numerical model that is able to validate the design rules of the booster vane in terms of bird strike robustness and investigate the possibilities of Variable Stator Vane (VSV) systems.

The validation of the numerical models for bird strike requires quantitative measurements. Strain gauges on one hand can tell something about local deformations at discrete points on a structure. The measurement of residual energy after impact [ref eigen werk] and reaction forces on the other hand are valuable parameters that give an idea of the global performance. Optical measurements can also provide full field displacement and strain fields. The optical view however is often disturbed in bird strike experiments, and a stereo set-up of high-speed cameras dedicated to the measurement would be required. The measurement of reaction forces therefore remains one of the primary parameters for characterizing the impact event. Several techniques were already successfully used, from ballistic pendulums to Hopkinson bars and load cells and methods in between.

The oldest technique is the ballistic pendulum. The original idea dates back from the reference work of Robins in 1742 [1], where it was used to measure the momentum of a bullet. An application of the pendulum in bird strike research can be found in the work of Bertke et al. [2], where a 5 wire pendulum was used to measure the total transferred momentum of a bird strike on titanium blades. They calculated the transferred momentum from the chord length and the oscillation period after impact.

Hopkinson introduced a first version of the Hopkinson bar in 1914 [3], which was basically an advanced version of the ballistic pendulum. Hopkinson proposed a co-axial system of two bars, where the second bar is suspended and able to trap a part of the momentum depending on its length. The strain waves in the first bar however can, in the ideal case, be directly related to the impact force, as was tried in the reference works on bird strike from Barber et al. [4] and Wilbeck [5], in which forces were measured of bird strike on flat and inclined surfaces using a Hopkinson bar set-up. But they had to integrate the momentum signals. Because of the high frequencies that were dispersed due to the large diameters of the bars, exact force time signals could not be obtained. A more recent attempt was taken in the work of Seidt [6].

In the work of Allcock [7], the targets were attached to a set of calibrated beams. The deflection of the target was measured, from which the impact force was derived. In more recent work [ref eigen werk], the targets were able to move in the direction of impact, from which the impact force could be derived directly.

To test bigger and complex full scale structures such as leading edge wings, flaps or windshields and to acquire force time signals, a set of load cells or instrumented links are often used to measure the reaction force at discrete points [8-16]. The problem with load cells is that the force signal is often influenced by vibrations of the supporting structure. Numerical simulations are capable of incorporating a part of the boundary conditions, but the interpretation of the signals is nevertheless not straightforward.

Prior to the booster vane experiments that were to be executed in the course of this project, the purpose was to develop a tool able to measure reaction forces in multiple directions. This is achieved by allowing movement of the set-up, which has the advantage to decouple the experiment from the environment to some extent and to guarantee safety. More specific, three rotational degrees of freedom are given to a well-chosen mass to acquire the transferred rotational momentum, which is an idea that originates from the work of Premont et al. [17] and Steinhagen et al. [18]. Premont and Steinhagen mounted vanes onto a rigid object that is able to pivot around one point, and measured the transferred momentum around three axes using accelerometers.

Contrary to the work of Premont and Steinhagen, the moment arm from the point of rotation to the impact location is much shorter, reducing the influence of Eigen frequencies of the force measurement tool. Also, the momentum in this work is derived optically from the images of one high speed camera (HSC). The HSC is already necessary to acquire the horizontal offset of the bird. A so-called cone structure was designed onto which multiple vane configurations can be mounted. To verify the set-up and to have an intermediate step between the initial calibration experiments [Ref eigen werk] and the booster vane experiments, a rigid steel vane was used as target object. This paper will introduce the cone as the tool to allow the rotational movement. The different steps necessary to derive the momentum of the cone will be explained in detail. Finally, some results will be shown as well as a comparison with a numerical model, using SPH modelling for the bird.

In the next section, the test set-up to launch the birds and the steel vane will be introduced. In section 3, the main principle of the force measurement with the cone will be explained. Section 4 contains the actual derivation of the rotational momentum. The next sections contain the results of some experiments, a comparison with simulations and finally a conclusion.

2) Test set-up

a. Ugent bird strike test set-up

The experiments were performed on the Ghent University bird strike set-up (Figure 1). The set-up is capable of shooting birds up to 42 kJ. Birds can be launched with a weight of maximum 4 lb (according to the regulations [19]) at speeds up to 250 m/s. At the beginning of each experiment, a projectile called a sabot is filled with foam in accordance to the desired shape, after which gelatine is moulded into the acquired foam shape. The sabot is mounted in front of a pressure vessel and released at the required pressure. After the release trigger, the sabot launches through a barrel and strips off from the bird in the stripper chamber using a cone shaped stripper, after which the stripped bird flies into the test chamber and impacts on the required target. Before each experiment, the test chamber is evacuated up to 0.2 bar absolute pressure to be able to perform precise velocity measurements.

Figure 1: Ghent University bird strike test set-up

b. Target: steel vane

The set-up to measure the transferred rotational momentum will be tested and validated using a simplified steel vane (Figure 2). Tests on the actual vanes cannot be disclosed. The vane consists of a V-shaped steel bar welded to a plate. The holes in the plate will be used to mount the vane to the cone structure. Making a (construction steel) vane with similar behaviour (in terms of elastic energy, deformation and thickness) as the Titanium vanes is almost impossible due to the difference in yield strength and stiffness.

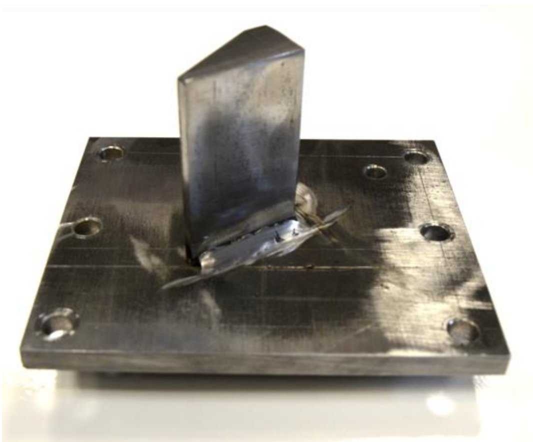

Figure 2: Simplified steel vane

The steel vane will serve as an intermediate step between the initial calibration experiments on rigid targets [Ref eigen werk] and the experiments on the booster vanes because it will combine a significant amount of change of momentum with the splitting of the bird and the surface over which mass is deflected is significantly shorter, as will also be the case in the booster vane experiments.

3) Principle rotational momentum measurement

In order to acquire reaction forces in multiple directions, multiple degrees of freedom (DOF) are necessary. It proved to be practically difficult to allow translational movement in multiple directions for impact measurements, which is why the idea of Premont et al. [17] and Steinhagen et al. [18] to use rotational DOFs was further investigated. Practically, the rotational DOFs are realized by a cone structure (Figure 3 shows the first version). The ball joint at the tip of the cone is the centre of rotation. The vane fixtures should be mounted on top of the flange attached to the cone. The rectangular shaped protrusions on each side of the flange are used for the optical measurements.

At impact, the cone structure with the vane fixture starts rotating around the ball joint. From this movement the momentum can be calculated. The weight and rotational inertia was designed in such a way that the displacement of the flange during impact is in the order of millimetres (1-5 mm), which minimizes the influence of the set-up on the experiment. This way the experiment is also decoupled from the environment as much as possible (the structure to hold the ball joint, which is assumed rigid sees no moment) and is therefore less dependent on supporting structures. The distance from the point of impact to the rotation point is also much larger than the radius of the ball joint, which decreases the possible influence of friction forces on the momentum measurement.

Figure 3: the cone structure

Newton’s second law for rotational systems is the following:

$$\tau = I\alpha$$

With τ, the torque in Nm, α, the rotational acceleration in rad/s^2 and I, the inertia tensor in kg.m^2, which can be obtained from CAD software (containing the parts with the actual dimensions):

$$I = \begin{bmatrix} I_{xx} & I_{xy} & I_{xz} \\ I_{xy} & I_{yy} & I_{yz} \\ I_{xz} & I_{yz} & I_{zz} \end{bmatrix}$$

The angular momentum L can be calculated by integrating the torque:

$$L = \int \tau \, dt$$

in kg.m^2 /s or also Nms.

The idea is to have a tool that does not influence the experiment. This means that, if the vane would be mounted on a rigid surface, the same impact forces should be measured. Applying this to the equations above, the angular momentum from the torque in an impact event with rigid boundary conditions obtained in equation 3 should give the same results as the angular momentum obtained from the rotational accelerations in equation 1:

$$L = \int I\alpha \, dt = I \int \alpha \, dt = I\omega$$

This is only valid when I is not dependent on time, or also, that the entire structure is rigid and fixed. This is why the displacement during impact should be limited. For deforming objects such as a booster vane, I is not exactly constant. But, simulations showed that the average transferred momentum is equal in both situations with and without cone, as well as the amplitude of the oscillations superimposed on this average value. Small delays in the momentum signals showed to be the biggest influence of the cone. The influence of the cone will be further discussed in the results section.

The fact that a well-designed inertial tensor does not influence the momentum transfer can ease the comparison with the simulations. It allows to make abstraction from the actual geometry in the simulation (bolts, accelerometers, stiffeners, little plates with optical patterns, etc.) to speed up the process of meshing and reduce the model size. While boundary and initial conditions are acquired from the actual experiment, the inertial tensor can be approximated in the numerical analysis, as schematically shown in Figure 4.

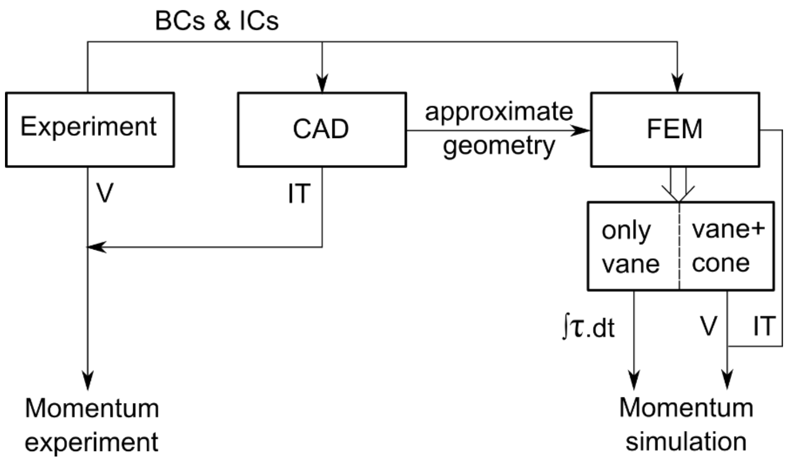

Figure 4: Comparison between experiment and simulation (IT: inertial tensor, V: rotation speed, τ: torque, BC: boundary condition, IC: initial condition)

The rotational momentum is a measure for the impact force and will be used to compare simulations and experiments because it is fairly independent of the set-up. If the actual impact forces would have to be calculated, the impact radius would need to be known which (a) is an estimation but worse, (b) is not constant through time and will therefore introduce another unknown and error in the process. Therefore, the momentum will remain the parameter for comparison throughout the remainder of this paper.

The next section will explain how the rotational speeds are derived.

4) Deriving the rotational speeds

a. Overview

As mentioned in the previous sections, the kinematics of the cone are derived from an optical measurement. Figure 5 shows the final concept of the cone including the steel vane with two strain gauges, indications on the flange to be able to set the initial position of the cone and two optical patterns at each side of the cone. On the right, the convention for the coordinate system is shown. The z-axis is aligned with the impact direction, the y-axis is aligned according to the axis of the cone or also the vertical upward direction and the x-axis completes the orthogonal right-handed coordinate system.

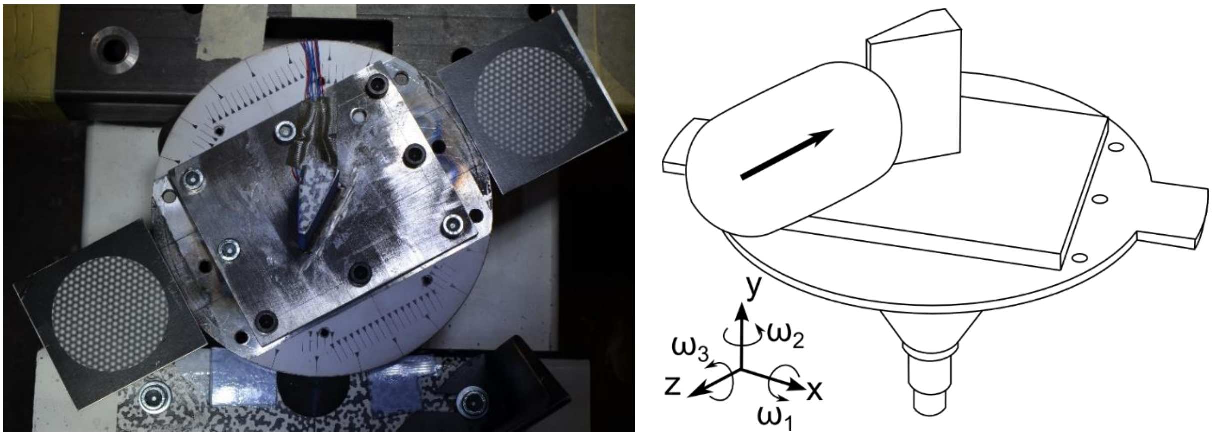

Figure 5: Cone set-up with steel vane and optical patterns (left) and convention of the coordinate system (right)

The displacements from the optical patterns are derived using a new Fourier based algorithm [Ref pattern paper?]. The main advantage above a correlation based technique is that it is very robust. During bird strike, a lot of debris, foam particles and pieces of bird fly above the patterns, which can introduce a lot of noise in the results and therefore requires a robust algorithm. The patterns move on a spherical path, which is a boundary condition to the problem and makes it possible to derive kinematics with only one camera. A schematic overview of how the kinematics are derived is shown in Figure 6.

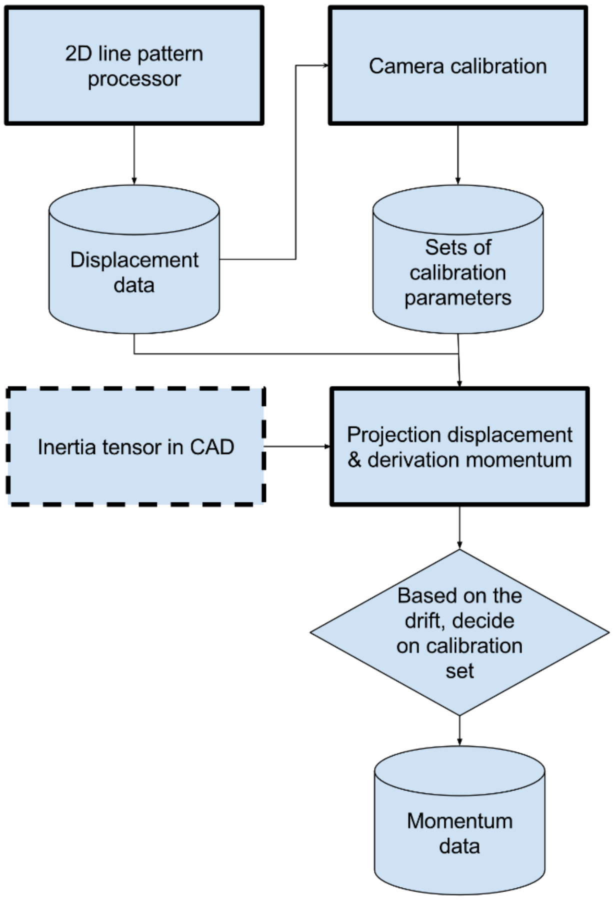

Figure 6: Schematic overview derivation cone kinematics

In a first step, the images are processed using the Fourier based technique [Ref pattern paper?]. The calculated displacements however are only a projection of the actual displacements of the patterns of the cone, so some transformation needs to be done. To be able to do this right, the extrinsic and intrinsic camera parameters need to be defined through camera calibration. An optimization procedure is used to calculate these parameters. The solution space proved to be very noisy with a lot of local optima, multiple sets of calibration parameters were therefore generated after which an additional parameter called the drift (which will be introduced further on) will decide on the final calibration set. Once this is done, the displacements can be projected onto the sphere (the spherical path on which the patterns move) and the rotational speeds and momentum can be calculated. In the following sections the main steps are described in more detail.

b. Calibration camera

The camera is calibrated using 15 points, partly on the cone, partly on the patterns. Specifying these coordinates in a world coordinate system and linking them to the corresponding image pixels makes it possible to calibrate the cameras using an optimization technique [20]. In this work, a pinhole camera model without distortion is assumed. To be able to link the world to the image coordinates, four transformations are needed (Figure 7): a transformation from the world to the camera coordinate system (3 translation and 3 rotation parameters), a projection on the CCD (1 parameter), a 180° rotation of the CCD and a shift of the image (1 parameter). All the parameters except for the last one are quite common. The last parameter is intrinsic to the high speed cameras (HSC's), as there is a limit to the amount of data the HSC can save in a certain amount of time. At higher framerates, the amount of pixel information or rather resolution is reduced. In this work, most experiments were recorded with a framerate of 27.000 fps, which resulted in a reduced resolution of 448x288 (compared to the full resolution of 1024x1024). For the Photron SA-4 cameras, the position of this smaller region (which will be further referred to as the region of interest or ROI) on the CCD is vertically in the middle of the CCD, while the position of the ROI in the horizontal direction can be chosen in steps of 32 pixels. This parameter was never noted in the experiments and is therefore an additional optimization parameter.

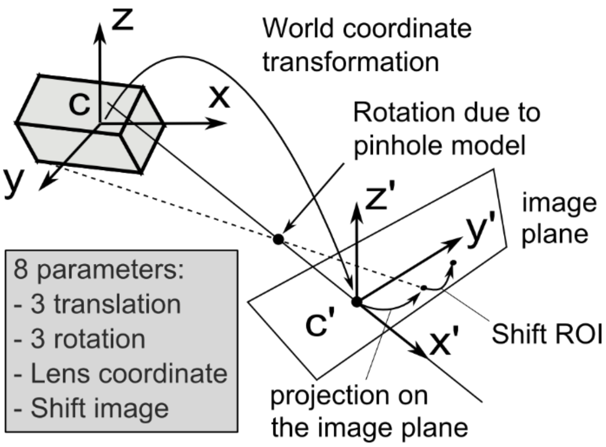

Figure 7: Transformations from world to CCD coordinates

A lot of optimization techniques exist. Essentially, they can be subdivided in local and global techniques. Local optimization starts from an initial guess or also set of parameters and tries to find the solution starting from this input vector. A global optimization scheme on the other hand tries to examine the entire solution space (in a clever way). In general, local optimization schemes are used for the calibration of the camera. Multiple experiments however showed that the solution of the local optimization is very dependent on the initial guess. Also with a global optimization scheme, different solutions were found each run, indicating that the solution space is very noisy with a lot of local optima. This phenomenon is partly the result of a poor set of almost coplanar calibration points, but also due to the nature of the problem. For each experiment, therefore, multiple calibration sets were generated. An additional parameter introduced in the next section was used to decide on the final calibration set.

For the optimization, the sum of the squares of the differences between the world coordinates projected on the image plane, and the corresponding actual image coordinates for each of the 15 points is minimized using a genetic algorithm in Matlab.

c. Calculation of the actual displacements

The displacements of the patterns are only a projection of the actual displacements. How the actual displacements are determined is shown in the schematic in the figure below. In the figure, each vector has an abbreviated name: cv stands for camera vector (starting from the centre of the pattern, pointing in the direction of the camera), pdv stands for projected displacement vector, this is the vector calculated by the pattern software, pv stands for position vector, this is the vector from the centre of rotation to the centre of a pattern. All the other vectors are derived from these three known vectors.

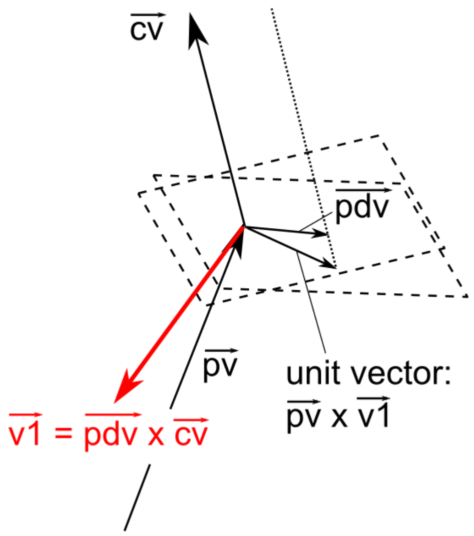

Figure 8: Calculation of the actual displacements

The camera vector can directly be derived from the calibration parameters. The projected displacement vector lies in the plane defined by cv, at an orientation which can also be determined from the calibration parameters. The initial position vector is defined by the initial position of the cone.

The actual displacement vector lies in the plane defined by pv (for small displacements, the displacement can be assumed tangential to the sphere’s surface), but also in the plane defined by cv x pdv. Therefore, first a vector v1 is created, after which the wanted unit vector is obtained from the cross product of pv and v1.

This procedure can be repeated for each time step to obtain the actual displacements of the centre of both patterns. The mean of those displacements (from both patterns) gives the displacement of the centre of the flange of the cone, from which the two main rotation components can be derived.

The calculation of the third rotation component along the axis of the cone makes use of the fact that this rotation is very small. The difference between the displacement of both patterns in the direction perpendicular to the axis of the cone and the vector between the patterns divided by the distance between the patterns gives a good estimate of the rotation about the cone's axis. From the displacements and rotations, the rotation speeds can be calculated. Together with the inertia tensor obtained from the CAD drawing, the momentum can be determined.

The calculation is separately done for each pattern. The rigid motion of the cone implies that the vector between both patterns should remain constant, but due to the fact that the whole structure is not perfectly rigid and due to errors in the optimization of the calibration parameters, this is not the case. Multiple tests however showed that the drift on the norm of this vector is a good measure for the quality of the calibration. From the different calibration sets that are generated with the global optimization scheme, the set with the least drift is therefore chosen.

d. Error quantification

The methodology to derive the momentum, including the calculation of the displacements of the patterns, the calibration of the cameras and the projection on the sphere was validated using a set of quasi-static and impact tests. For these experiments, speckle patterns were attached to the cone and vane and tracked with a stereo DIC set-up. DIC or digital image correlation is a speckle pattern tracking method with sub-pixel accuracy, which results in high resolution full-field displacement and strain maps. The tracking is done by correlating small parts of the subsequent images called subsets, each containing an almost unique set of speckels [21]. The orientations derived from these DIC measurements were a reference to calculate the errors, because DIC is a well-known technique that can be used in a stereo set-up to directly acquire 3D displacements and includes a distortion model. From these experiments, it could be deduced that the errors were in general less than 5%. In Figure 9, the results of the two main axes of a static experiment are shown. In this quasi-static test, the cone was rotated manually. The time scale is a fictitious one corresponding with one image per second. To the left, the error on the displacements can be seen (cut off for low displacements). To the right, the rotational speeds are shown. The figures show that good correlation is achieved.

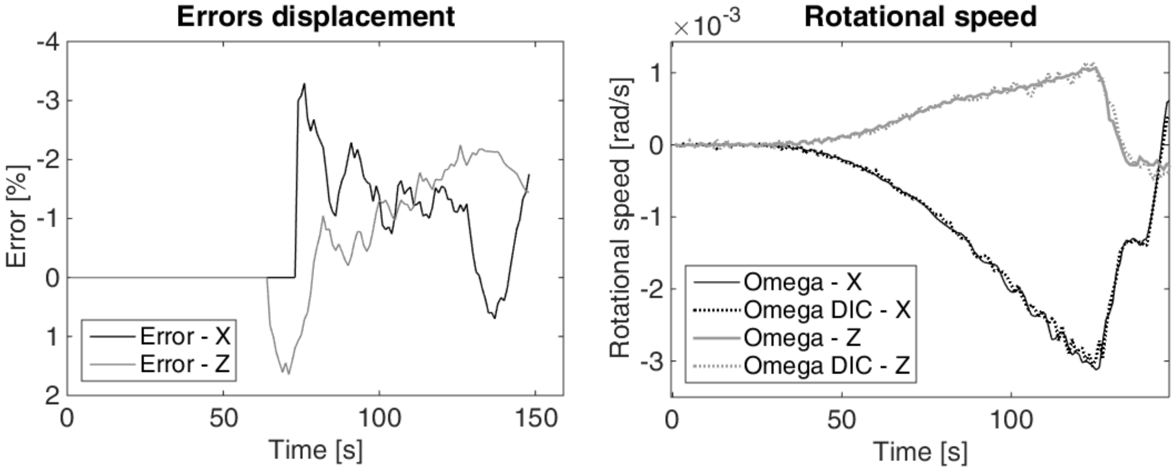

Figure 9: Errors and rotational speeds of a quasi-static test

5) Results

a. Impact test

In this section, the results of two bird strikes with the same impact conditions will be shown. Two tests were executed with a gelatin bird of 300 gram with a gelatin mixing ratio of 1:6 at an impact speed of approximately 110 m/s. The initial position of the cone was twice 30 degrees turned to the left.

In Figure 10, three subsequent high speed images are shown of both tests (a top view, where the bird comes from the bottom of the image). The total ROI of 448x288 pixels is shown. Little space is foreseen to make sure that patterns are always in the ROI throughout the entire movement of the cone. In the third image, the bird has travelled through its own length, while the movement of the cone can barely be seen.

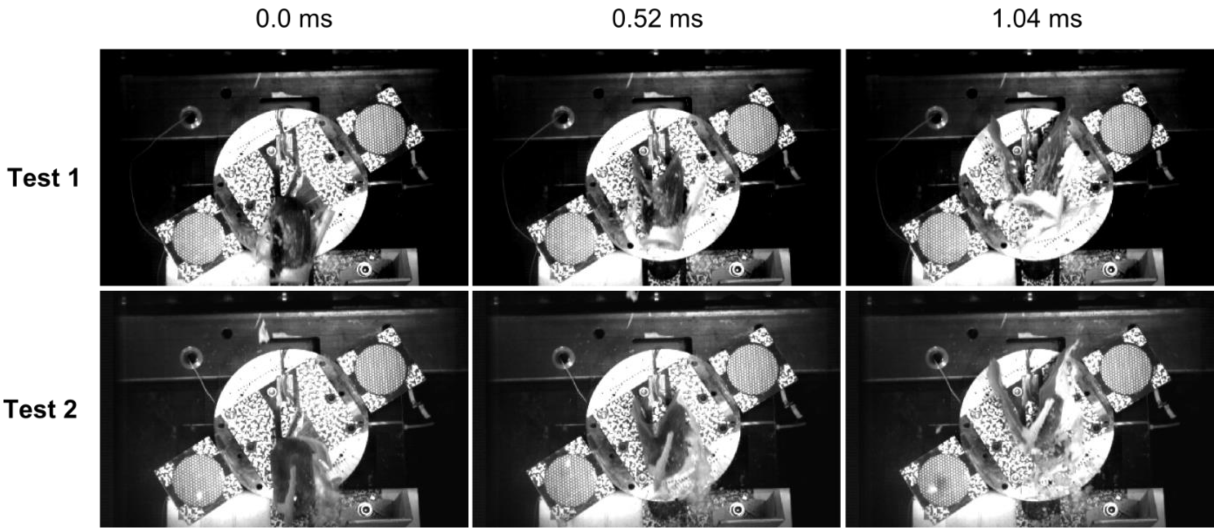

Figure 10: High speed images of two bird strikes with similar impact conditions on the steel vane mounted on the cone set-up.

For both tests, multiple calibration sets are generated, from which the one with the least drift is chosen (being 0.25 and 0.27 mm peak to peak respectively). The displacements from the patterns are projected on the spherical path and the rotational speeds are calculated. The entire structure is drawn in Solid Works to extract the inertial tensor. From the rotational speeds and the inertial tensor, the momentum is calculated. To get a better relative comparison and to take the different speed and mass of both birds into account, the calculated momentum of the cone is divided by the initial momentum of the bird. To get a better overview of the results, a low pass filter of 3 kHz was applied. The result of this process is shown in Figure 11.

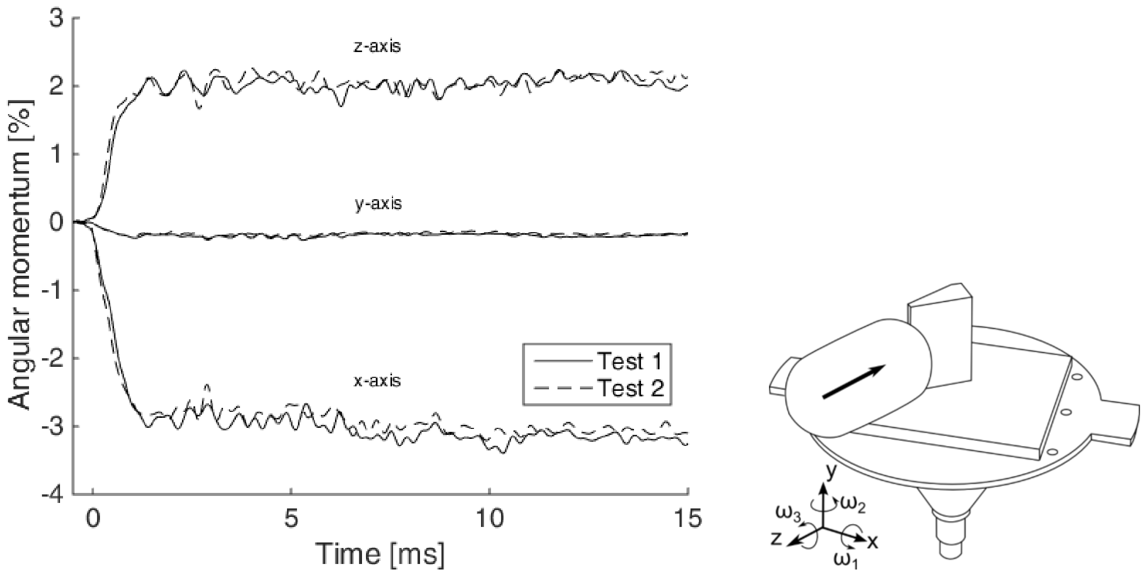

Figure11: Normalized momentum data test 1 and 2

The two tests give very similar results, for all the three axes. Most of the mass is deflected to the right (positive x-axis), which makes the cone move to the left and back (the negative x- and z-axis). This corresponds with a positive and negative rotational momentum around the z-axis and x-axis respectively. The magnitude of the momentum around the z-axis is smaller than around the x-axis because some mass is also deflected to the left (negative x-axis). The rotational momentum around the y-axis is a lot smaller because the radius of the impact force with respect to the axis of the cone is a lot smaller than for the other axes. The sign is negative because most of the deflection happens at the front of the steel vane, which is positioned slightly to the left of the axis of the cone from the point of view of the bird.

b. Correlation with a numerical model

An explicit simulation was ran with the same impact conditions as test 2, where the bird was modelled with smoothed particle hydrodynamics or SPH. SPH is increasingly used in bird strike simulations as it already proved to be quite capable of simulating high deforming matter with defragmentation [22]. Also, tracking of field values is not a problem for SPH. A complete and clear explanation of SPH and its governing equations can be found in literature [23]. A structured mesh is generated based on the shape of the mould, with a slight offset to exactly match the mass with the experiments. The impact position is derived from the high speed images as best as possible (both in the vertical as the horizontal direction).

For the numerical model, the cone was modelled as a deformable object, able to rotate around the tip of the cone. The vane was modelled as accurately as possible, including the welds and membranes for the strain gauges. Both the cone and the vane were modelled with reduced integration hexahedral elements.

A linear Mie-Gruneïsen EOS is used for the bird material model, which relates the pressure to the density. Parameters for porcine gelatine were found in literature (c0 = 1570 m/s and s = 1.77) [24], which is very similar to water. The bird was tilted 8° in the vertical plane to have a better match with the impact conditions of the experiment.

Figure 12 shows a qualitative comparison from the top view of the cone. The difference in time should be 0.05 ms maximum.

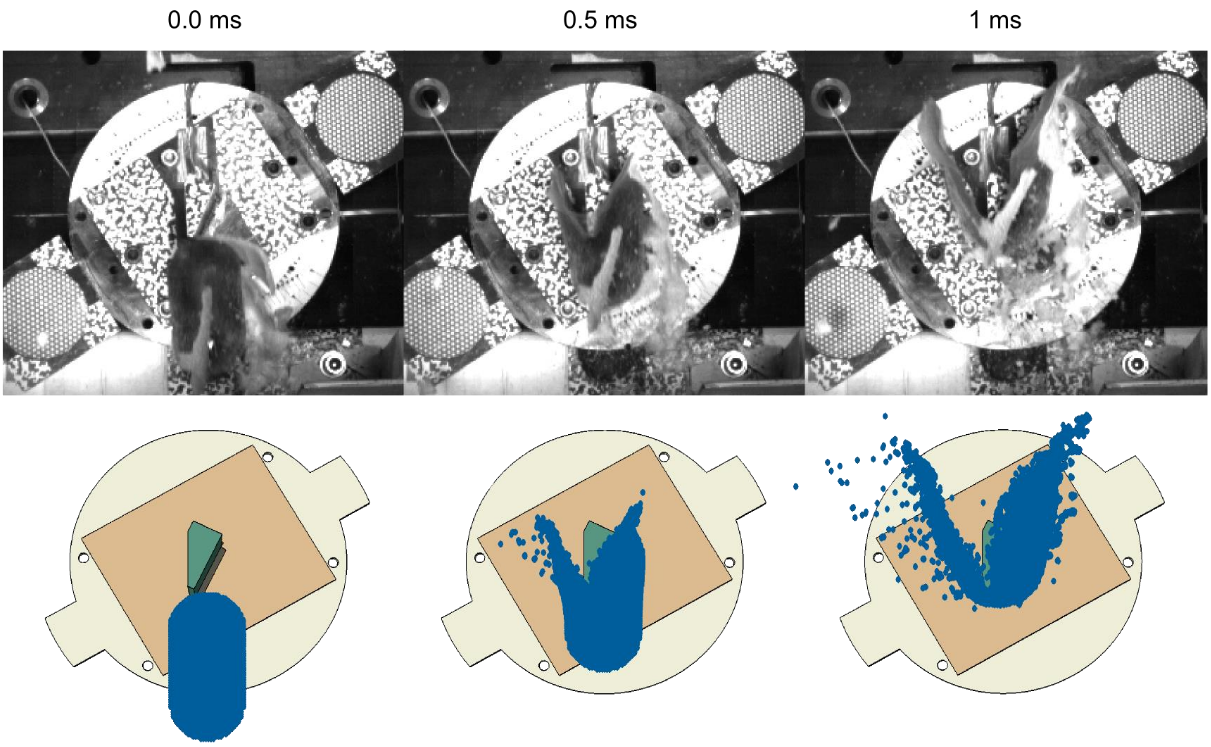

Figure 12: Qualitative comparison between experiment and simulation

The global behaviour correlates well with the experiment. Both the direction in which the mass is deviated as the speed of the deviated mass after impact.

Figure 13 shows a comparison between the momentum obtained from the simulation and from the experiments, including a 2mm offset on the estimation of the impact location both in the negative as the positive x-direction in the simulation. For the momentum of the simulation, the speeds are extracted at two locations on the cone. Together with the inertia tensor from the model, the momentum can be obtained.

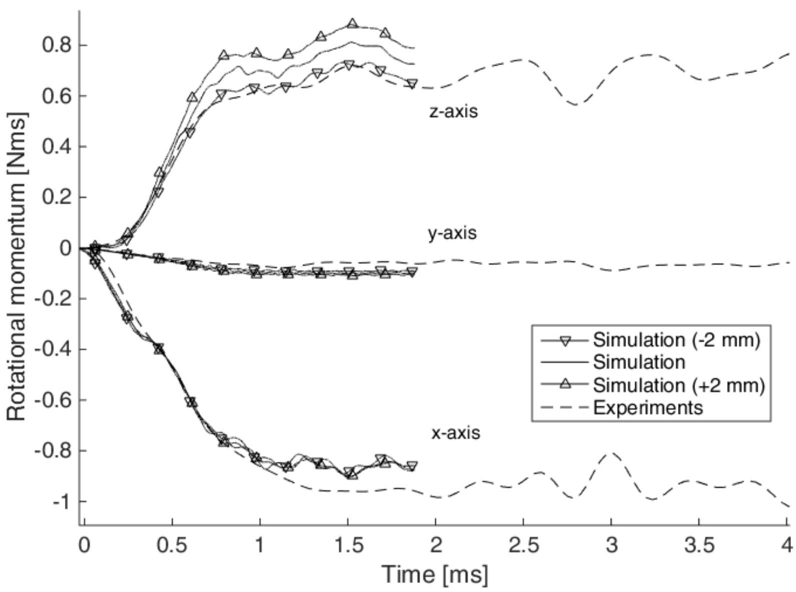

Figure 13: Comparison of the rotational momentum in the simulation and the experiment

The impact location of the bird is crucial. A 2mm offset error for example, which can be easily made, corresponds with 4.5% of the bird mass that is deviated in the other direction. This kind of error is therefore most represented in the momentum around the z-axis. The order of magnitude of momentum transfer is approximated well, but some differences can be observed. In the simulation, the momentum transfer to the x-axis is slightly lower. The graphs also shows that possibly, an error of approximately 2mm was made in the estimation of the x-offset. The momentum transfer around the x-axis also takes slightly longer in the experiment.

A comparison between the strain in the simulation and experiment at the back and the left side is shown in Figure 14. The influence of the offset is less pronounced in the strain signals. The left strain gauge measures the deformation along the weak axis of the steel vane and therefore sees more strain. For the left strain gauge, the strain amplitude is 15-20% higher in the simulation. And after 0.6 ms, the correlation with the strain gauge at the back gets worse. Apart from that, the response of the vane is capture quite well.

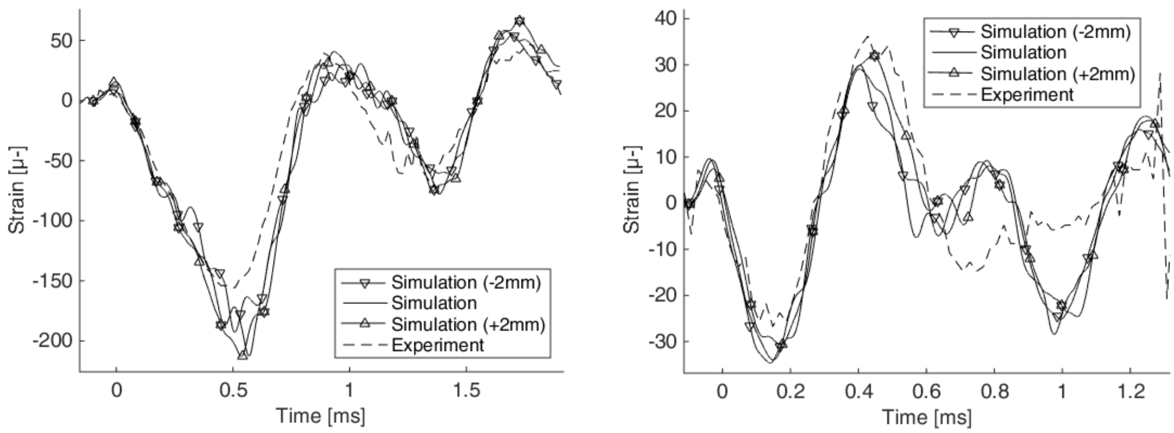

Figure 14: Comparison of the strain at the left side (left) and the back (right) of the vane in the simulation and the experiment

c. Influence of the cone

To show that the influence of the cone is negligible (Figure 15), a reference simulation with and without cone is performed as well. For the simulation without cone, the ties that connected the vane to the cone are connected instead to a fixed reference point. The forces and moments acting on this reference node are recorded throughout the simulation.

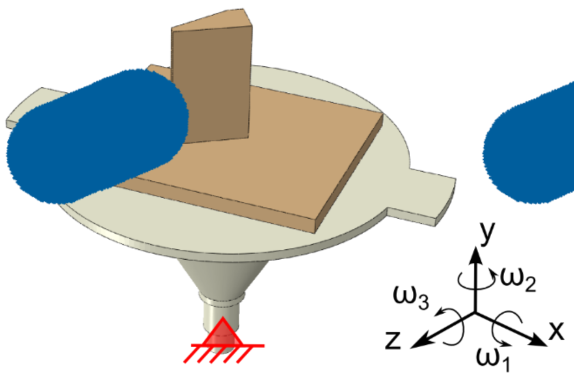

Figure 15: Simulation with and without cone

In a post processing step, the forces and moments are transformed to the actual location of the ball joint (with respect to the vane), integrated over time (as in equation 3) and plotted together with the momentum obtained from kinematics of the simulation with the cone shown in the previous section. The results are depicted in Figure 16.

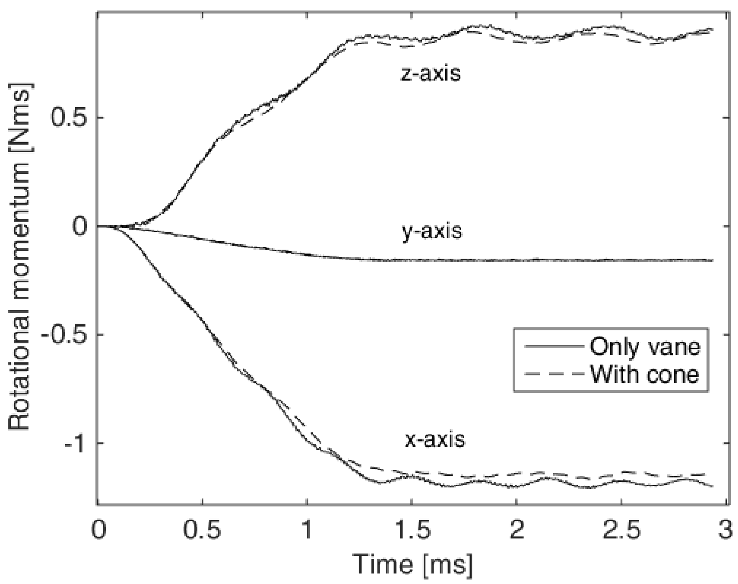

Figure 16: Comparison rotational momentum with and without cone (simulation)

It can be observed that the transferred momentum is comparable. The momentum transfer is slightly lower with cone, but still sufficiently small compared to other errors sources.

6) Conclusion

In this paper, the development and results of a multi-axial momentum measurement tool are discussed. The multi-axial force measurement is realized using a well-chosen mass in the shape of a cone which is able to rotate freely around the tip of the cone. The ability to rotate freely makes it possible to determine the transferred rotational momentum. This requires that the kinematics of the cone, obtained from an optical measurement in three main steps: calculation of the projected displacements from the optical patterns, calibration of the camera using a global optimization technique and transformation of the projected displacements on the spherical path on which the optical patterns move.

Quasi-static and impact tests show that the developed tool can be used to get a reliable estimate of the transferred rotational momentum. Two bird strike tests with the same impact conditions are compared and give very comparable momentum transfer results. A numerical simulation of one of these tests (using SPH for the bird) shows a good correlation in terms of momentum. Finally, simulations indicate that the tool has a negligible influence on the experiment for the considered stiff steel vane. The tool proved to be very useful and successful results have been obtained for multiple sets of real Titanium vanes.

Acknowledgements

The authors would like to thank Techspace Aero for the cooperation throughout the project. The research leading to these results has received funding from the European Union’s Seventh Framework Programme FP7/2007-2013 under grant agreement n_ ACP2-GA-2012-314366-E-BREAK. More information can be found at http://www.e-break.eu/.

References

1. Robins, B., *New principles of gunnery: containing the determination of the force of gun-powder and an investigation of the difference in resisting power of the air to swift and slow motions.*1742.

2. Bertke, R.S. and J.P. Barber, *Impact Damage on Titanium Leading Edges From Small Soft-Body Objects*, 1979, University of Dayton Research Institute: Dayton, Ohio.

3. Hopkinson, B., *A Method of Measuring the Pressure Produced in the Detonation of High Explosives or by the Impact of Bullets.* Philosophical Transactions of the Royal Society of London A: Mathematical, Physical and Engineering Sciences, 1914. **213**(497-508): p. 437-456.

4. Barber, J.P., H.R. Taylor, and J.S. Wilbeck, *Bird impact forces and pressures on rigid and compliant targets*1978, Wright-Patterson Air Force Base, Ohio; Alexandria, Va.: Air Force Flight Dynamics Laboratory, Air Force Systems Command ; Distributed by Defense Technical Information Center, Defense Logistics Agency.

5. Wilbeck, J.S., L. Air Force Materials, and L. Air Force Wright Aeronautical, *Impact behavior of low strength projectiles*1978, Wright-Patterson Air Force Base, Ohio: Air Force Materials Laboratory, Air Force Wright Aeronautical Laboratories, Air Force Systems Command.

6. Seidt, J.D., et al., *Dynamic Load Measurement of Ballistic Gelatin Impact Using an Instrumented Tube*, in *XII International Congress and Exposition on Experimental and Applied Mechanics*2012.

7. Allcock, A.W.R. and D.M. Collin, *The Development of a Dummy Bird for Use in Bird Strike Research*1969: H.M. Stationery Office.

8. McCarthy, M.A., et al., *Modelling of Bird Strike on an Aircraft Wing Leading Edge Made from Fibre Metal Laminates – Part 2: Modelling of Impact with SPH Bird Model.* Applied Composite Materials, 2004. **11**(5): p. 317-340.

9. Guida, M., *Study, design and testing of structural configurations for the bird-strike compliance of aeronautical components*, in *PhD thesis*, U.o. Naples, Editor 2008: Italy.

10. Guida, M., et al., *Analysis of Bird Impact on a Composite Tailplane Leading Edge.* Applied Composite Materials, 2008. **15**(4-6): p. 241-257.

11. Georgiadis, S., et al., *Bird-strike simulation for certification of the Boeing 787 composite moveable trailing edge.* Composite Structures, 2008. **86**(1–3): p. 258-268.

12. Guida, M., et al., *Certification by birdstrike analysis on C27J fullscale ribless composite leading edge.* International Journal of Impact Engineering, 2013. **54**: p. 105-113.

13. Zhu, S., et al., *Numerical Simulation of Bird Impact on Fibre Metal Laminates.* Polymers & Polymer Composites, 2014. **22**(2): p. 147-156.

14. Liu, J., Y. Li, and X. Gao, *Bird strike on a flat plate: Experiments and numerical simulations.* International Journal of Impact Engineering, 2014. **70**: p. 21-37.

15. Anghileri, M. and G. Sala. *Theoretical assessment, numerical simulation and comparison with tests of birdstrike on deformable structures*. in *Proceedings of the 20th ICAS congress*. 1996. Sorrento, Italy.

16. Kermanidis, T., et al., *Development and Validation of a Novel Bird Strike Resistant Composite Leading Edge Structure.* Applied Composite Materials, 2005. **12**(6): p. 327-353.

17. Premont, E.J. and K.R. Stubenrauch, *Impact Resistance of Composite Fan Blades*, 1974, Aircraft Engine Group, General Electric Co.: Cincinnati, Ohio. p. 1-143.

18. Steinhagen, C.A. and C.T. Salemme, *The Impact Resistance of Current Design Composite Fan Blades Tested Under Short Haul Operating Conditions*, 1973, General Electric Company: Evendale, Ohio. p. 1-67.

19. *EASA Certification Specifications*. 2015; Available from: http://easa.europa.eu/document-library/certification-specifications.

20. Hartley, R. and A. Zisserman, *Multiple View Geometry in Computer Vision*2003: Cambridge University Press. 700.

21. Sutton, M.A., J.-J. Orteu, and H. Schreier, *Image Correlation for Shape, Motion and Deformation Measurements: Basic Concepts,Theory and Applications*2009: Springer Publishing Company, Incorporated. 364.

22. Heimbs, S., *Computational methods for bird strike simulations: A review.* Computers & Structures, 2011. **89**(23-24): p. 2093-2112.

23. Liu, G.R. and M.B. Liu, *Smoothed particle hydrodynamics : a meshfree particle method*2003, New Jersey: World Scientific. xx, 449 p.

24. Shepherd, C.J., et al., *The Dynamic Behaviour of Ballistic Gelatin.* AIP Conference Proceedings, 2009. **1195**(1): p. 1399-1402.